

24 June 2008
Draft Version

Is there evidence for X-ray emitting plasma very close to the photospheres of O stars?

Maurice A. Leutenegger^{1,2,3,4}

¹ *Laboratory for High Energy Astrophysics, Code 662, NASA/Goddard Space Flight Center, Greenbelt, MD 20771*

² *Department of Physics and Astronomy, Swarthmore College, Swarthmore, PA 19081*

³ *Department of Physics and Columbia Astrophysics Laboratory, Columbia University, 550 West 120th Street, New York, NY 10027*

⁴ *NASA Postdoctoral Fellow*

Submitted 2008 Xxxxx XX

ABSTRACT

I describe a procedure for accurately assessing parameter confidence limits for low signal-to-noise X-ray emission line complexes in which the blending of Doppler-broadened lines is significant. I apply this methodology to measure the f/i ratios of high-Z He-like ions in the X-ray spectra of several O stars. I find that the data in question actually provide *no significant constraint on the location of the X-ray emitting plasma*. This is not surprising, as the data are of poor statistical quality. These data thus do not require a two-component model for the origin of O-star X-ray emission, and do not present a near-star high-ion problem, as suggested in Waldron & Cassinelli (2007). This is consistent with earlier results, using lower-Z He-like ions, constraining the bulk of the X-ray emitting plasma to be distributed throughout the wind and not near the photosphere. It is also consistent with the consensus finding that emission lines from high-Z ions in the spectra of many O stars have significant Doppler broadening, which is not expected for lines forming very close to the photosphere.

Key words:

stars: early type — star: winds, outflows — techniques: spectroscopic — methods: data analysis

1 INTRODUCTION

The first high resolution X-ray spectra of O stars obtained by the diffraction grating spectrometers onboard *XMM-Newton* and *Chandra* showed He-like triplet emission with strong intercombination lines (i) and weak or absent forbidden lines (f). This was initially surprising; many researchers were familiar with the idea that this was a signature of a high-density plasma, and the densities implied would have been difficult to understand if they were present in the winds of O stars, where the X-rays are thought to originate. In their investigation of the RGS spectrum of ζ Puppis, Kahn et al. (2001) showed that the observed line ratios were due to the strong ultraviolet radiation from the photosphere, which excites electrons from the metastable $1s2s\ ^3S_1$ state (the upper level of the forbidden line) to the $1s2p\ ^3P_J$ states (the upper levels of the intercombination lines). The dependence of the f/i ratio on the UV field was in fact derived in the first works on this subject (Gabriel & Jordan 1969; Blumenthal et al. 1972), but, in the absence of an obvious context for its importance, it was less widely appreciated than the density dependence. The dependence of the observed ratio on the strength of the UV field allowed Kahn et al. (2001) to use

the ratios to infer rough plasma locations. They found that X-rays were indeed originating from the wind of ζ Pup.

Waldron & Cassinelli (2001) subsequently used the formalism of Gabriel & Jordan (1969) and Blumenthal et al. (1972) to derive relatively precise radii of formation from the observed f/i ratios for ζ Orionis, under the assumption of a single formation radius for a given ion. They found that most of the X-ray emitting plasma was located at radii consistent with a wind-shock origin. However, one of the more perplexing results of this investigation was the inference from the f/i ratio of Si XIII of the presence of hot X-ray emitting plasma very close to the photosphere of ζ Ori (at a height of less than 0.1 stellar radii). Cassinelli et al. (2001) made a similar inference based on the f/i ratio of S XV observed in the X-ray spectrum of ζ Pup, and Waldron et al. (2004) again found this behavior for S XV and Ar XVII in the X-ray spectrum of Cyg OB2 8A. Again, in each of these cases, the bulk of the X-ray emission was found to originate from locations consistent with shocks distributed in the wind, while only the highest-Z He-like ions were inferred to be forming near the photosphere.

Although the initial prediction of X-ray emission from

O stars based on the observed super-ion states was couched in the context of a base coronal model (Cassinelli & Olson 1979), both the UV observations of super-ions and the subsequent detection of X-rays from O stars (Harnden et al. 1979; Seward et al. 1979) indicate nothing about the mechanism of X-ray production. Moderate resolution X-ray spectra obtained with the *Einstein* Solid State Spectrometer showed that at least the soft X-ray emission must be distributed in the winds of O stars and cannot be located in a corona or other confined region near the photosphere (Cassinelli & Swank 1983). Around the same time, it was proposed by Lucy & White (1980) that the instability of the radiative driving mechanism of O star winds leads to the formation of shocks which are capable of producing X-ray emission throughout the winds of O stars. A large body of theoretical work has further developed this idea (e.g., Lucy 1982; Macfarlane et al. 1993; Cooper 1994; Cooper & Owocki 1994; Feldmeier et al. 1997,?; Owocki & Cohen 1999).

Although a few OB stars with anomalous X-ray emission properties show clear evidence of the interaction of their stellar winds with large scale magnetic fields (Cohen et al. 2003; Gagné et al. 2005, e.g.), the spectra of most O stars observed with the diffraction grating spectrometers onboard *XMM-Newton* and *Chandra* are consistent with the wind-shock paradigm for X-ray plasma formation. The strongest single piece of evidence for this is the dramatic velocity broadening of the emission lines (including the lines of the He-like triplets); they typically have HWHM of order half the wind terminal velocity, or about 1000 km s^{-1} (e.g., Kahn et al. 2001; Cassinelli et al. 2001; Kramer et al. 2003; Cohen et al. 2006). This is in contrast with coronal sources, which never have velocity broadening or shifts that are detectable at the resolution of the current generation of instruments ($\gtrsim 100 \text{ km s}^{-1}$; in a few cases it is possible to detect orbital motion in close binaries, but this can barely be resolved). Although there are still unsettled questions in the interpretation of O star line profiles, especially regarding the relative importance of mass-loss rate reduction, porosity, and resonance scattering (e.g., Owocki & Cohen 2001; Ignace & Gayley 2002; Kramer et al. 2003; Oskinova et al. 2004; Cohen et al. 2006; Owocki & Cohen 2006; Oskinova et al. 2006; Leutenegger et al. 2007), there is no doubt that the non-negligible line widths should be interpreted in the context of some kind of wind-shock model.

The presence of any X-ray emitting material close to the stellar photosphere of a “normal” O star would be difficult to explain in the context of a wind-shock model. Numerical hydrodynamic simulations of instabilities in radiatively driven stellar winds indicate that several tenths of a stellar radius are required to allow the instabilities to develop (e.g., Owocki et al. 1988) if the line-driving instability is self-excited; the presence of perturbations at the base of the wind might alleviate the problem to some degree, but generating X-rays very close to the photosphere (less than a tenth of a stellar radius) would likely still be a problem (Feldmeier 1995). However, note that numerical simulations give no indication that the characteristic shock velocity scales with the local flow velocity, as suggested by Waldron & Cassinelli (2001), Cassinelli et al. (2001), and Waldron & Cassinelli (2007). On the contrary, these simulations typically show reverse shocks caused by rapidly accelerating flows colliding with clumps that follow the trajectory of the mean wind

velocity law, with large shock velocities even for the shocks occurring closest to the star (Owocki et al. 1988; Feldmeier 1995; Runacres & Owocki 2002).

The inference of X-ray emitting plasma forming close to the photospheres of the O stars ζ Ori (Waldron & Cassinelli 2001), ζ Pup (Cassinelli et al. 2001), and Cyg OB2 8A (Waldron et al. 2004) led Mullan & Waldron (2006) to suggest the possibility of a two-component origin for their X-ray emission, with the bulk of the X-ray emission arising from shocks distributed throughout a wind flowing from the equator, but with the highest temperature plasma originating in polar coronal loops very close to the photosphere. The high-ion f/i ratios which led to the inference of X-ray emitting plasma close to the stellar photospheres of those stars are the strongest piece of observational evidence presented in support of this scenario.

In Leutenegger et al. (2006), my collaborators and I attempted to reproduce some of these early results and found that the f/i ratios of Si XIII in the X-ray spectrum of ζ Ori and S XV in the spectrum of ζ Pup did not require the presence of hot plasma very close to the photosphere, but were consistent with formation radii several tenths of a stellar radius above the photosphere at the 68% confidence level. We identified two main sources of error in those measurements of characteristic radii of formation by Waldron & Cassinelli (2001) and Cassinelli et al. (2001) that indicated the existence of X-ray emitting plasma close to the photosphere: the measurements of the line ratios themselves, and the model photospheric UV flux shortward of the Lyman break, which is relevant for Si XIII and higher-Z He-like ions.

Recently, Waldron & Cassinelli (2007) (hereafter WC07) have published measurements of line ratios as well as velocity shifts and widths for a large sample of O stars observed with the *Chandra* High Energy Transmission Grating Spectrometer (HETGS). Using f/i line ratios, they have inferred radii of formation near the photosphere for high-Z helium-like ions observed in the spectra of a number of stars (typically S XV or Si XIII), and they have characterized their observations as constituting a near-star high-ion problem. The fact that this behavior is observed for a large sample of stars lends greater weight to the claim of a universal problem than observations in only three stars. If their observations were confirmed, they would present a significant challenge to the wind-shock mechanism for producing X-rays from O stars.

WC07 have published an erratum in which they have made significant corrections to the line ratio measurements and their confidence intervals. In particular, due to a bug in their line-fitting code, the confidence intervals published in their original work were significantly underestimated. Furthermore, they revised their fit parameter confidence intervals from 90% to 68%. However, they report in the erratum that this does not affect their general conclusion that there is a near-star high-ion problem. I discuss their measurements in more detail in § 3.

In this paper I attempt to reproduce the measurements which lead WC07 to infer radii of formation near the photosphere for high-Z ions. In all cases that I consider, I find that the data provide no significant constraint on the radii of formation. However, this does not invalidate measurements for lower-Z ions, including those of WC07, which have generally found that those ions are *not* located near the photosphere.

This paper is organized as follows. In § 2 I give a brief review of the atomic physics of He-like triplets and the $\mathcal{R} \equiv f/i$ ratio. In § 3 I summarize the f/i ratio measurements of WC07. In § 4 I discuss the reduction of the data, present my measurements of f/i , and discuss possible explanations for the discrepancies between my results and those of WC07. In § 5 I discuss my results and give my conclusions.

2 RELATION BETWEEN PLASMA FORMATION RADIUS AND F/I RATIO

In this section I give a brief review of the behavior of the $\mathcal{R} \equiv f/i$ ratio of a He-like ion in the presence of a strong external UV field, as in the wind of an O-star. For a more complete discussion, see e.g. Leutenegger et al. (2006). I use the notation of that paper throughout. In particular, I adopt the use of script \mathcal{R} to denote the f/i ratio, and italic R to denote quantities comparable to a stellar radius.

The diagnostic utility of this ratio originates in the fact that the upper level of the forbidden line (f), $1s2s^3S_1$, is metastable. If a process excites electrons in this state to the upper levels of the intercombination lines (i), $1s2p^3P_{1,2}$, the f/i ratio is altered. The criterion for significant alteration of the line ratio is that the excitation rate from $1s2s^3S_1$ to $1s2p^3P_{1,2}$ should be comparable to the decay rate of $1s2s^3S_1$ to ground.

There are two processes that can excite electrons in this way: electron impact excitation, and photoexcitation. The former becomes important at high density, the latter when the UV field intensity J_ν is strong.

The \mathcal{R} ratio is an especially powerful diagnostic because the decay rate to ground of the upper level of the forbidden line is a strong function of Z , so that even though the range of Z typically observed only spans factor of two, the range of densities or UV field strengths probed by the observed \mathcal{R} ratios spans a few orders of magnitude.

Gabriel & Jordan (1969) and Blumenthal et al. (1972) solved the rate equations to show that

$$\mathcal{R}(\phi, n_e, T) = \mathcal{R}_0(T) \frac{1}{1 + \phi/\phi_c + n_e/n_c(T)}, \quad (1)$$

where $\mathcal{R} \equiv f/i$; \mathcal{R}_0 is the ratio in the limit of low UV field strength and low density; ϕ is the photoexcitation rate from $1s2s^3S_1$ to $1s2p^3P_J$; n_e is the electron density; and ϕ_c and n_c are the ‘‘critical’’ photoexcitation rate and density, respectively, where \mathcal{R} drops to half of \mathcal{R}_0 . ϕ_c , n_c , and \mathcal{R}_0 are functions of atomic parameters. n_c and \mathcal{R}_0 depend weakly on temperature.

In the case of an ion in a O-star wind, the value of ϕ is proportional to the geometrical dilution $W(r) = \frac{1}{2}\{1 - [1 - (R_*/r)^2]^{1/2}\}$, and the density is negligible in comparison with the critical density, so we may write

$$\mathcal{R} = \mathcal{R}_0 \frac{1}{1 + 2PW(r)} \quad (2)$$

where P is a constant that depends only on atomic physics and the photospheric UV flux. By assuming that emission from a given ion comes from a single radius, one may invert this expression for an observed value of \mathcal{R} to find a characteristic radius of formation; this is the approach taken by WC07. Other approaches based on more realistic assumptions may be taken to extract information regarding the

radial location of the plasma (e.g., assuming a radially distributed plasma, as in Leutenegger et al. 2006).

The theory developed in Gabriel & Jordan (1969) and Blumenthal et al. (1972) is adequate for most practical applications. However, it does not include the effect of blended dielectronic recombination (DR) satellite lines from Li-like species, which can be important for high-Z He-like ions. Given that the temperature distribution of X-ray emitting plasmas observed on O stars is skewed to lower temperatures, this effect is likely significant for Si XIII and higher-Z ions.

In § 4, I will show that the f/i ratios I measure in this paper are poorly constrained, and in all cases I consider (with one exception) the 90% confidence intervals do not exclude $\mathcal{R} = \mathcal{R}_0$, and the data thus do not constrain the plasma formation radius. Thus, I will not use the formalism described in this section to calculate allowed ranges of plasma formation radii. This formalism has, however, been used to calculate the radial dependence of \mathcal{R} in Leutenegger et al. (2006), in which meaningful constraints on the f/i ratios for other He-like triplets were measured.

For purposes of this paper, it is sufficient to note that the satellite lines will lower the effective observed value of \mathcal{R}_0 for high-Z ions. This effect has been included in the calculations of Porquet et al. (2001), but unfortunately the highest-Z ion considered in that work is Si XIII. Thus, for Si XIII, I adopt $\mathcal{R}_0 = 2.3$ from Porquet et al. (2001); for S XV, I adopt $\mathcal{R}_0 = 2.0$ from Blumenthal et al. (1972); and for Ar XVII, I interpolate the Blumenthal et al. (1972) values for S XV and Ca XIX and take $\mathcal{R}_0 = 1.7$. Because they do not include DR satellites, the \mathcal{R}_0 values of Blumenthal et al. (1972) for high-Z ions are probably overestimated by at least 10%, but given the low precision of the measurements considered in this paper, that is an adequate level of accuracy. All of the values of \mathcal{R}_0 adopted were evaluated at T_m , the temperature of maximum line power. In reality, the lines are almost certainly formed at lower temperatures, given the dominance of low temperatures in the observed differential emission measure distributions. The effect of this assumption on the adopted values of \mathcal{R}_0 is likely to be small.

3 SUMMARY OF F/I RATIO MEASUREMENTS IN WC07

In § 3.1 I present a summary of the measurements of WC07 implying the formation of X-ray emitting plasma close to the photospheres of some O stars. In § 3.2 I discuss their fitting method and error analysis procedures.

3.1 Measurements

In Table 1 I have collected all f/i ratios reported in WC07 which led them to infer plasma formation radii close to the stellar surface. For purposes of this paper, I have chosen the criterion that the reported upper limit to the plasma location is $< 1.7R_*$ at 68% confidence. The results given are from the erratum of WC07 and not from the original publication.

This does not imply that X-ray emitting plasma as distant as $1.7R_*$ would necessarily be problematic if it were detected. As discussed in the introduction, numerical modeling

of the line-driving instability indicates that a wind seeded with perturbations could develop strong shocks significantly lower than $1.5 R_*$. The choice to include data constraining X-ray emitting plasma to be closer than $1.7 R_*$ is made to ensure that all data indicating a possible near-star high-ion problem are examined.

I only show results for Si XIII and S XV, and not for lower-Z ions. I also give the results of Waldron et al. (2004) for Ar XVII in the spectrum of Cyg OB2 8A, which indicate that this ion is also formed close to the photosphere for this star.

WC07 report separate measurements using the Medium Energy Grating (MEG) and High Energy Grating (HEG), rather than fitting MEG and HEG data simultaneously. The MEG and HEG are similar transmission gratings with a factor of two difference in dispersion; all HETGS observations give simultaneous MEG and HEG spectra. The HEG and MEG results are both given for every ion considered, when available. In cases where measurements from one grating imply formation close to the photosphere while those from the other do not, I give both for comparison, although there is no reason to suppose that MEG and HEG data should give results whose differences are statistically significant.

Of the measurements listed in Table 1, three show consistent results for both the MEG and HEG measurements, two show marginally consistent results, two were only made with the MEG and not with the HEG, and one shows inconsistent results between the MEG and HEG, given the reported 68% confidence intervals.

In Table 1 I also report the total number of counts in the fit range for each complex for both the HEG and the MEG. Although some of the complexes have a significant number of counts, some of them have so few counts that it is hard to see how one could extract any meaningful information from them other than the overall normalization. For example, the S XV triplet of ζ Ori has a total of only 24 counts (MEG and HEG combined), of which about half are expected to be distributed between the forbidden and intercombination lines, with the remainder being in the resonance line.

Of the 17 stars considered in WC07, ten show no evidence requiring X-ray emitting plasma close to the photosphere (Cyg OB2 9, δ Ori, ϵ Ori, HD 150136, ι Ori, β Cru, 9 Sgr, 15 Mon, ζ Oph, and τ Sco), while seven stars have some evidence requiring this. In each of these seven cases, only the highest-Z He-like species observed shows any evidence requiring X-ray emitting plasma close to the photosphere, except in the case of Cyg OB2 8A, for which both S XV and Ar XVII require this, and σ Ori, for which both Mg XI and Si XIII require this.

Three He-like complexes that were claimed to require X-ray emitting plasma close to the photosphere in the original version of WC07 (S XV in the spectrum of ζ Oph, and Si XIII in the spectra of ι Ori and ζ Ori) are no longer claimed to require this in the erratum. This is particularly significant in the case of ζ Ori. The formation radius of Si XIII inferred by Waldron & Cassinelli (2001) for this star was the origin for the first claim of a near-star high-ion problem, and led Waldron & Cassinelli (2001) to infer that some of the X-ray emitting plasma was located close enough to the photosphere that high-density effects might become important. This claim is implicitly rescinded by the new measurements of WC07 published in their erratum: the HEG data now

give no constraint, and the MEG data give a *lower* limit of $R > 1.8 R_*$.

3.2 Fitting method and error analysis

In this section I give a brief summary of the methodology of WC07 based on their original publication, the erratum, and private communications from W. Waldron.

The data in the spectral region of each He-like complex are modeled by three Gaussian emission lines plus a continuum component. Each Gaussian has its own normalization, but they all share the same centroid Doppler shift, and the same Doppler width.

The data are fit by finding the point in model parameter space that minimizes the statistic

$$\chi^2 = \sum_i \frac{(N_i - M_i)^2}{\sigma_i^2}, \quad (3)$$

where i are the indices of spectral bins, N_i are the observed counts in each bin, M_i are the predicted model counts, and σ_i are the variances associated with the observed counts. The variances are computed using

$$\sigma_i = \max[1.87, \sqrt{N_i}], \quad (4)$$

This function has similar behavior to the Gehrels variance function (Gehrels 1986),

$$\sigma_i = 1 + \sqrt{0.75 + N_i}, \quad (5)$$

which can be used in XSPEC or other similar spectral fitting programs.

It is not clear how parameter confidence intervals were computed in WC07. The standard way to estimate model parameter errors is to vary the parameters and compare the change in fit statistic due to the variation (e.g. Lampton et al. 1976; Press et al. 2007, ‘‘Confidence Limits on Estimated Model Parameters’’, Chapter 15.6 in Numerical Recipes).

For example, to find the confidence intervals for \mathcal{R} , one could vary \mathcal{R} about the best-fit value while allowing the other parameters to also vary to minimize the fit statistic. To obtain confidence intervals of 68.3%, 90%, and 95.4% one would find the interval on which the fit statistic increased by 1.0, 2.706, and 4.0, respectively.

If one were using the normalizations of f and i as free parameters rather than \mathcal{R} , one could construct a two-parameter confidence region. Here the contours of 68.3%, 90%, and 95.4% confidence would be defined by delta-fit-statistics of 2.30, 4.61, 6.17, respectively. Then one would find the values of the f/i ratio allowed from this plot.

Because the confidence intervals reported by WC07 for \mathcal{R} are symmetric about the best-fit value, it seems likely that they were not obtained using a delta-fit-statistic criterion, which will produce quite asymmetric confidence intervals (see § 4.5 for further discussion). Rather, they may have been computed using some other algorithm which finds a single relative error for each model parameter, perhaps based on the signal-to-noise ratio of the data.

If such an algorithm was used, it is difficult to see how it could properly account for the covariance of the line normalizations with other parameters. Specifically, the derived normalization of the intercombination line is very sensitive

Table 1. Measured \mathcal{R} ratios reported in WC07 that imply formation radii close to the photosphere

Star	Ion	MEG			HEG		
		\mathcal{R}^a	R^b	N^c	\mathcal{R}^a	R^b	N^c
Cyg OB2 8A	Ar XVII ^d	< 0.16	~ 1.0	64	0.43 ± 0.37	~ 1.0	53
Cyg OB2 8A	S XV	0.74 ± 0.34	< 1.14	140	0.87 ± 0.37	< 1.26	90
ζ Pup	S XV	0.60 ± 0.62	< 1.48	85	0.79 ± 0.65	< 1.84	46
θ^1 Ori C	S XV	1.32 ± 0.66	< 4.88	495	0.70 ± 0.25	< 1.04	365
ζ Ori A	S XV	0.77 ± 1.21	< 1.66	17	—	—	7
σ Ori	Si XIII	0.21 ± 0.37	< 1.02	25	—	—	17
HD 206267	Si XIII	0.34 ± 0.32	< 1.52	59	1.97 ± 1.71	≥ 1.02	25
ξ Per	Si XIII	2.35 ± 1.06	> 1.90	209	0.30 ± 0.26	< 1.12	89

^aMeasured $\mathcal{R} \equiv f/i$ ratio with 68% confidence limits.

^bInferred radius of formation (R_*).

^cTotal number of counts in the MEG and HEG spectra in the fit range considered (without rebinning or subtracting background). Note that this includes all three lines in the complex (r , i , and f), but that only about half of the counts are in the f and i lines, which give the \mathcal{R} ratio.

^dFrom Waldron et al. (2004).

This table reports measured \mathcal{R} ratios and inferred radii of formation from the erratum of WC07. These values are significantly different than those in the original article

to the strength and width assumed for the forbidden line. In order to properly account for this, it is necessary to make a two-parameter confidence region for the normalizations of the forbidden and intercombination lines while allowing all the other fit parameters to vary as well.

A further potential problem with the methodology of WC07 is the use of the Doppler shift of the complex as a free parameter. Because the number of counts is small in many of the complexes considered, and the complexes have significant blending, a significant Doppler shift in the centroid can be degenerate with other model parameters. Furthermore, the centroid Doppler shift is expected to be close to zero, based on the profiles of stronger lines in the same part of the spectrum. I discuss this further in § 4.4.

4 DATA REDUCTION AND ANALYSIS

In § 4.1 I describe the reduction of the *Chandra* data used in this paper. In § 4.2 I describe the Gaussian fitting procedure used throughout this section. In § 4.3 I use this procedure to fit the data using a standard, robust procedure and find the 90% confidence intervals for all interesting parameters, as well as 68%, 90%, and 95% confidence intervals for \mathcal{R} . In the remainder of this section I discuss possible fitting artifacts and systematic errors.

4.1 Data reduction

All of the data considered in this paper are from archival *Chandra* HETGS (Canizares et al. 2000) observations of O stars. I give a list of all observations used in Table 2.

The level one event files were reprocessed with `acis_process_events` to add up-to-date CTI corrections, after which the data were reprocessed with standard CIAO routines for HETG spectra, producing spectrum and background histograms, as well as response matrices and ancil-

Table 2. List of observations with net exposure times

Star	obsid ^a	t^b
Cyg OB2 8A	2572	65.1
ζ Pup	640	67.6
θ^1 Ori C	3, 4	49.5, 30.9
ζ Ori A	610, 1524	59.6, 13.8
σ Ori	3738	91.0
HD 206267	1888, 1889	34.1, 39.5
ξ Per	4512	158.8

^a*Chandra* Observation ID.

^bNet exposure time in ks.

lary response files. CIAO 3.4 and CalDB 3.3.0 were used in all cases.

Fitting was performed simultaneously on both gratings (HEG and MEG) on both positive and negative first orders and using all available observations, with no coadding or rebinning; the one exception to this is θ^1 Ori C, where I fit the two observations separately, as the magnitude of its X-ray emission is known to be rotationally modulated (Gagne et al. 1997). The use of unrebinned data is appropriate, since I use the C statistic and not χ^2 (Cash 1979).

The procedures described in the preceding paragraphs are essentially identical to those described in the data analysis threads on the CIAO webpage¹.

4.2 Gaussian fitting procedure

In all cases, I used a model with five free parameters. Three parameters give the line normalizations: $\mathcal{R} \equiv f/i$, $G = (f + i)/r$, and the overall normalization of the complex. The other two parameters are the Doppler widths and shifts of the

¹ <http://cxc.harvard.edu/ciao/threads/>

Gaussians, which were constrained to be the same for all lines in a complex. In all cases except where explicitly stated, the Doppler shift was fixed to zero. This is done to avoid fitting degeneracies, and because the shift is expected to be very close to zero for the complexes considered. I discuss the assumption of zero Doppler shift in more detail in § 4.4.

The fitting procedure I used is similar to the approach taken by WC07, but with the important difference that I used the line ratios and overall complex normalization as free parameters rather than the individual line normalizations of f , i , and r . This does not significantly affect the *best-fit* values, but it greatly simplifies the extraction of confidence regions for the parameter of interest, \mathcal{R} , using the delta-fit-statistic criterion (Lampton et al. 1976; Press et al. 2007). I emphasize that this procedure is identical to that of WC07 in the sense that I am fitting three Gaussian emission lines with the same velocity broadening and shift, and the only difference is in the set of parameters I use as independent variables.

Because f and i are blended due to both the finite resolution of the spectrometer and Doppler broadening, the normalizations of f and i have significant covariance. One will underestimate the uncertainty on \mathcal{R} if one simply adds errors on the individual line normalizations in quadrature while ignoring the covariance. However, when using \mathcal{R} explicitly as a model parameter, its uncertainty can be computed directly by calculating the change in fit statistic obtained by varying it, thus bypassing the issue of evaluating the covariance of the individual lines.

Another possible approach (not taken in this paper) would be to use the individual line normalizations as free parameters rather than the \mathcal{R} and G ratios, and then to construct two-parameter confidence regions for the normalizations of the forbidden and intercombination lines. The line ratio allowed for a given confidence level could be found from the allowed region on this plot.

I do not subtract background in any fits. The most rigorous way to include the effects of background would be to model the observed background spectrum and then add the modeled background into the total model for the source region. However, the number of background counts in the wavelength regions containing the He-like triplets is very small and can be adequately modeled as an addition to the weak bremsstrahlung continuum. As a representative example, based on the number of counts observed in the background spatial region from 4-6 Å, I estimate the number of background counts in the source extraction region of ζ Ori near the S XV triplet to be 0.48 ± 0.07 for the coadded first-order MEG data and 0.68 ± 0.08 for the coadded first-order HEG data, which is small compared with the observed number of source counts in S XV of 17 in the MEG and 7 in the HEG. The other data sets have comparable or greater source count rates. Thus, I take the approach of treating the background as a weak contaminant to the continuum, which is dominated by bremsstrahlung.

I approximate the sum of the continuum and background as a power-law of index two (which is flat when plotted in flux per unit wavelength vs. wavelength), with the normalization determined from a separate fit to the spectrum near the complex of interest; moderately strong lines are excluded from the continuum fit. This procedure is slightly different from that of WC07, who subtract the background

and model the continuum as bremsstrahlung from a 10 MK plasma. However, given the small number of counts observed in each complex and the small spectral regions used in the fits, a power law of index two will characterize the continuum and background accurately enough to give equivalent results.

In all cases, the He-like triplets were fit over a fixed range: 3.9-4.05 Å for Ar XVII, 4.99-5.15 Å for S XV, and 6.59-6.79 Å for Si XIII.

4.3 Fit results

I have fit all of the complexes given in Table 1 according to the procedure outlined in section 4.2. In Tables 3 and 4 I present the results of the fits. Table 3 gives best-fit models with 90% confidence limits for individual parameters. In Table 4 I present 68%, 90%, and 95% confidence intervals for \mathcal{R} .

The results presented in Tables 3 and 4 are in some sense a different measurement than that reported in WC07; I have performed a joint fit to the combined MEG and HEG data (but without coadding), while WC07 performed separate fits to the MEG and HEG data. In order to facilitate a direct comparison of results, I have also fit the MEG and HEG data separately. I report the best-fit values and the 68%, 90%, and 95% confidence intervals on \mathcal{R} in Tables 5 and 6. The results presented in Tables 3, 4, 5, and 6 are compared to the results of WC07 in Figures 1, 2, and 3.

It should be noted that there is in general no astrophysical reason or instrumental to expect the MEG and HEG fits to give different results from each other or from a joint fit, and that I perform fits to the individual MEG and HEG data only in order to ensure a fair comparison of fit results. To the extent that one might expect instrumental differences between results from the different gratings, the best practice is to identify specific cases where discrepancies exist, not just between the MEG and HEG, but between positive and negative dispersion orders. In cases where there is a discrepancy, one can attempt to resolve it or to discard data that may be compromised. In cases where there is no discrepancy, one should perform a joint fit to maximize the statistical robustness of the results. In § 4.7 I examine individual grating orders for the few cases that do show a discrepancy between HEG and MEG results.

Although \mathcal{R} is constrained to be less than \mathcal{R}_0 at 68% confidence from the joint fits in a few cases, I find that this is true for only one case at 90% confidence: the Si XIII complex of ξ Per. I discuss this in more detail in § 4.8. Because all of the data considered (excepting ξ Per) are consistent with $\mathcal{R} = \mathcal{R}_0$ at 90% confidence, this implies that *these data cannot provide an upper limit to the plasma radial location* at 90% confidence.

Comparing the measurements of \mathcal{R} ratios made using only the MEG or only the HEG, I find significant, systematic disagreement with the best-fit values and confidence intervals reported by WC07 for several cases. However, in two cases (the HEG measurement of Si XIII for ξ Per, and the MEG measurement of Si XIII for σ Ori) I find nominal agreement with the measurement by WC07 of a small value of \mathcal{R} . These cases are considered in more detail in § 4.7.

As a visual check on the validity of my models, I present the data for two He-like triplets as representative examples

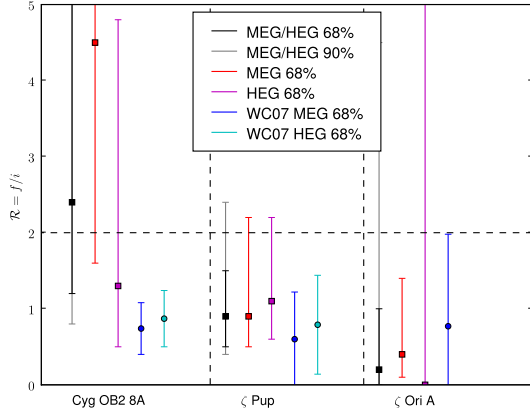
24 June 2008
 Draft


Figure 1. Comparison of several measurements of \mathcal{R} for S XV observed in several stars. Measurements are at 68% confidence, with 90% confidence also given in gray for my joint fit to the HEG and MEG data. My measurements were made using the maximum likelihood method (C statistic). The dashed line indicates the value of \mathcal{R}_0 for S XV. The black points give \mathcal{R} from my joint fits to MEG and HEG data, the red and magenta points give \mathcal{R} from individual fits to MEG and HEG data, respectively, and the blue and cyan points give \mathcal{R} from the individual fits of WC07 to MEG and HEG, respectively.

in Figures 4, 5, 6, and 7. I have overplotted the best-fit models (red), as well as models with \mathcal{R} taking the extreme values allowed at 90% confidence (blue and green), or $\Delta C = 2.706$. It is difficult to believe that any of the models presented are excluded at greater than 90% confidence, as would be predicted by the reported confidence intervals of WC07. In particular, the model for the S XV triplet of Cyg OB2 8A with $\mathcal{R} = \infty$ shows that it is possible to fit a model to this data set which has *no intercombination line*, with the broadening of the forbidden and resonance lines accounting for the observed counts near the wavelength of the intercombination line. According to the fit results of WC07, this model should be strongly excluded. (This should not be taken to imply that there is no intercombination line flux, which would be a surprising result not predicted by atomic theory, but rather that the data are of poor statistical quality and do not even exclude a model with no intercombination line flux.)

4.4 The effects of assumptions on velocity broadening and shifts on fit results

The fact that in some cases I have measured significantly different best-fit values and confidence intervals for \mathcal{R} than WC07 demands explanation. Unfortunately, WC07 have not reported enough information to quantitatively reproduce their results. Although they report best-fit values with 68% confidence limits for $\mathcal{R} \equiv f/i$ and $G \equiv (f+i)/r$, they do not report velocity widths or shifts. However, it is possible to test hypotheses regarding the origin of some of the discrepancies.

The greatest discrepancy between my measurements and those of WC07 is in the S XV triplet of Cyg OB2 8A. A clue to a possible source for this disagreement can be found in their reported $G \equiv (f+i)/r$ ratios. Using the MEG,

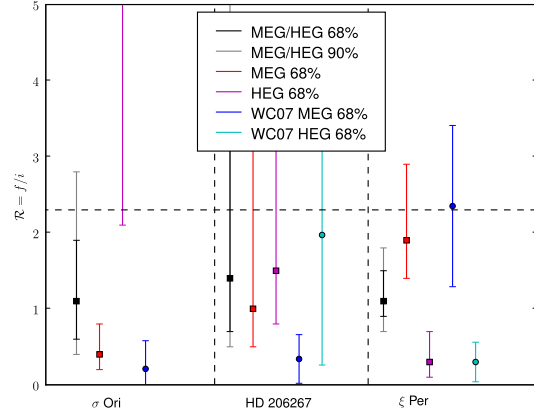


Figure 2. Same as Figure 1, but for Si XIII.

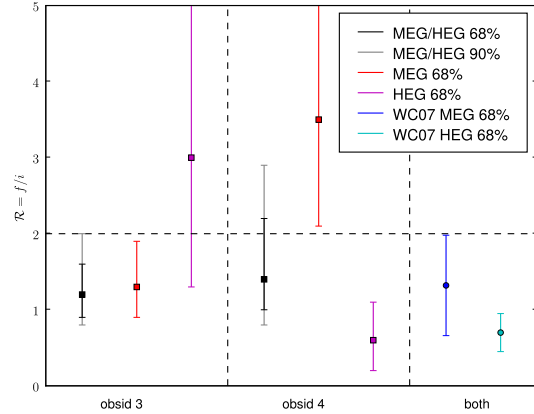


Figure 3. Same as Figure 1, but showing results for S XV in the spectrum of θ^1 Ori C. My fits were done for obsid 3 and 4 separately, while those of WC07 were done for coadded data.

WC07 measured $G = 3.16 \pm 1.70$, and using the HEG, they measured $G = 1.98 \pm 1.57$ (both at 68% confidence). In comparison, I measured $G = 0.8_{-0.3}^{+0.5}$ at 90% confidence. The best-fit value I found is much closer to the range expected from atomic physics ($G \sim 1.0$, e.g. Pradhan 1982; Porquet et al. 2001). Furthermore, the visual appearance of the data (shown in Figs. 4 and 5) suggests that $G \sim 1$ and not that $G \sim 3$.

One possible way to get a larger value for G would be to assume a significant blueshift in the line wavelengths, in which case one would be effectively counting photons near the rest wavelength of the resonance line as intercombination line photons. This would then increase the model value of i and decrease the model value of r . As discussed in § 4.2, I have assumed zero velocity shift in my fits. I have done this because one expects velocity shifts of zero for lines where the wind optical depth is small, and because I wanted to minimize the number of free parameters to avoid degeneracy.

To test this idea, I have fit models to the MEG and HEG data where \mathcal{R} and G were forced to take on the values reported by WC07. I allowed both the velocity width and the

Table 3. Best fit models for He-like triplets using maximum likelihood method

Star	Ion	\mathcal{R}	G	σ^a	n^b	C	bins
Cyg OB2 8A	Ar XVII	(0.8)	$0.7^{+2.2}_{-0.6}$	950^{+850}_{-400}	$8.1^{+3.9}_{-2.8}$	159.5	176
Cyg OB2 8A	S XV	> 0.8 (2.4)	$0.8^{+0.5}_{-0.3}$	950^{+250}_{-200}	41^{+6}_{-7}	196.5	188
ζ Pup	S XV	$0.9^{+1.5}_{-0.5}$	$0.8^{+0.5}_{-0.3}$	700^{+200}_{-200}	26^{+5}_{-4}	174.8	188
θ^1 Ori C (obsid 3)	S XV	$1.2^{+0.8}_{-0.4}$	$0.8^{+0.2}_{-0.2}$	350^{+100}_{-100}	99^{+10}_{-15}	265.4	188
θ^1 Ori C (obsid 4)	S XV	$1.4^{+1.4}_{-0.6}$	$0.8^{+0.4}_{-0.3}$	299^{+50}_{-50}	76^{+11}_{-16}	205.2	188
ζ Ori A	S XV	< 4.5 (0.2)	$0.4^{+0.8}_{-0.3}$	350^{+350}_{-250}	$2.5^{+1.4}_{-1.1}$	111.7	376
σ Ori	Si XIII	$1.1^{+1.7}_{-0.7}$	$1.0^{+0.5}_{-0.5}$	< 350 (200)	$2.3^{+0.9}_{-0.6}$	119.7	236
HD 206267	Si XIII	> 0.5 (1.4)	$0.7^{+0.5}_{-0.4}$	700^{+300}_{-250}	$5.5^{+1.3}_{-1.2}$	256.0	472
ξ Per	Si XIII	$1.1^{+0.7}_{-0.4}$	$1.2^{+0.5}_{-0.3}$	700^{+200}_{-100}	$9.5^{+1.1}_{-1.1}$	263.6	236

^aBest-fit Gaussian velocity width in units of km s^{-1} .

^bBest-fit normalization in units of 10^{-6} photons cm^{-2} s^{-1} .

All confidence intervals reported in this table are 90%, or $\Delta C = 2.706$. Parentheses denote a value that minimizes the fit statistic C where the parameter is either unconstrained at 90% confidence or gives only an upper or lower limit.

Table 4. Allowed ranges for \mathcal{R} at different confidence levels

Star	Ion	best fit	68.3%		90%		95.4%	
			min	max	min	max	min	max
Cyg OB2 8A	Ar XVII	0.8	0.1	3.3	0	∞	0	∞
Cyg OB2 8A	S XV	2.4	1.2	10.7	0.8	∞	0.7	∞
ζ Pup	S XV	0.9	0.5	1.5	0.4	2.4	0.3	3.5
θ^1 Ori C (obsid 3)	S XV	1.2	0.9	1.6	0.8	2.0	0.7	2.2
θ^1 Ori C (obsid 4)	S XV	1.4	1.0	2.2	0.8	2.9	0.7	3.4
ζ Ori A	S XV	0.2	0	1.0	0	4.5	0	∞
σ Ori	Si XIII	1.1	0.6	1.9	0.4	2.8	0.3	3.7
HD 206267	Si XIII	1.4	0.7	3.2	0.5	∞	0.4	∞
ξ Per	Si XIII	1.1	0.9	1.5	0.7	1.8	0.7	2.0

velocity shift to be free. The results are reported in Table 7. I find that models requiring their reported best-fit values of \mathcal{R} and G indeed prefer large blueshifts.

Since many emission line profiles in the X-ray spectra of O-stars are indeed quite blueshifted, especially for stars with high mass-loss rates, it is reasonable to ask whether the S XV triplet of Cyg OB2 8A might in fact be significantly blueshifted. One would expect an insignificant blueshift because of the relatively small atomic opacity of the wind at 5 Å. However, the most reliable way to test the expected blueshift is to fit the profile of a strong line nearby in the spectrum.

In Table 8, I report the results of a Gaussian fit to the Si XIV Ly α line of Cyg OB2 8A. I indeed find that the blueshift is consistent with zero, and that the velocity broadening is consistent with the measured value from my fit to S XV. Therefore, at least in this case, my assumptions about the velocity structure of S XV appear to be justified, and any fit to S XV which prefers a large blueshift must be regarded as an artifact.

Although it is not possible to know what fitting procedure led WC07 to obtain the results they report for Cyg OB2 8A, it seems reasonable to assume that allowing the velocity shift to be free may have led to degeneracy in model parameters. However, I have shown that fixing the velocity shift to zero is a good assumption, and that under this as-

Table 7. Best-fit velocity parameters assuming line ratios reported by WC07 for S XV in the spectrum of Cyg OB2 8A

Grating	\mathcal{R}	G	σ^a	Δv^b	n^c
MEG	(1.07)	(3.16)	1450	-725	39
HEG	(1.13)	(1.98)	325	-700	41

^aBest-fit Gaussian velocity width in units of km s^{-1} .

^bBest-fit velocity shift in units of km s^{-1} .

^cBest-fit normalization in units of 10^{-6} photons cm^{-2} s^{-1} .

Parentheses denote fixed parameters taken from WC07.

sumption, I find much more reasonable best-fit values for G . If this is indeed the case, then the low values of \mathcal{R} reported by WC07 for S XV in the spectrum of Cyg OB2 8A are likely an artifact of a fitting degeneracy.

4.5 Asymmetry of confidence limits on \mathcal{R} for S XV in the spectrum of ζ Pup

I find moderate disagreement with WC07 in the size of the error bars and the best-fit values of \mathcal{R} obtained using fits to only the MEG or HEG data. I also find that the confidence regions on \mathcal{R} are quite asymmetric, in contrast with the

Table 5. Allowed ranges for \mathcal{R} from fitting only the MEG data

Star	Ion	best fit	68.3%		90%		95.4%	
			min	max	min	max	min	max
Cyg OB2 8A	Ar XVII	0.2	0	1.0	0	∞	0	∞
Cyg OB2 8A	S XV	4.5	1.6	∞	1.0	∞	0.8	∞
ζ Pup	S XV	0.9	0.5	2.2	0.3	8	0.2	∞
θ^1 Ori C (obsid 3)	S XV	1.3	0.9	1.9	0.7	2.6	0.7	3.2
θ^1 Ori C (obsid 4)	S XV	3.5	2.1	6.6	1.6	12	1.3	23
ζ Ori A	S XV	0.4	0.1	1.4	0	3.5	0	6.2
σ Ori	Si XIII	0.4	0.2	0.8	0.1	1.3	0.1	1.8
HD 206267	Si XIII	1.0	0.5	3.4	0.3	∞	0.2	∞
ξ Per	Si XIII	1.9	1.4	2.9	1.1	4.2	1.0	5.6

Table 6. Allowed ranges for \mathcal{R} from fitting only the HEG data

Star	Ion	best fit	68.3%		90%		95.4%	
			min	max	min	max	min	max
Cyg OB2 8A	Ar XVII	1.9	0.2	∞	0	∞	0	∞
Cyg OB2 8A	S XV	1.3	0.5	4.8	0.2	∞	0	∞
ζ Pup	S XV	1.1	0.6	2.2	0.4	6.0	0.2	∞
θ^1 Ori C (obsid 3)	S XV	3.0	1.3	∞	0.9	∞	0.8	∞
θ^1 Ori C (obsid 4)	S XV	0.6	0.2	1.1	0.1	1.7	0.1	2.0
ζ Ori A	S XV	0	0	∞	0	∞	0	∞
σ Ori	Si XIII	6.7	2.1	∞	1.2	∞	0.9	∞
HD 206267	Si XIII	1.5	0.8	3.5	0.5	7.0	0.4	12
ξ Per	Si XIII	0.3	0.1	0.7	0.0	1.0	0.0	1.3

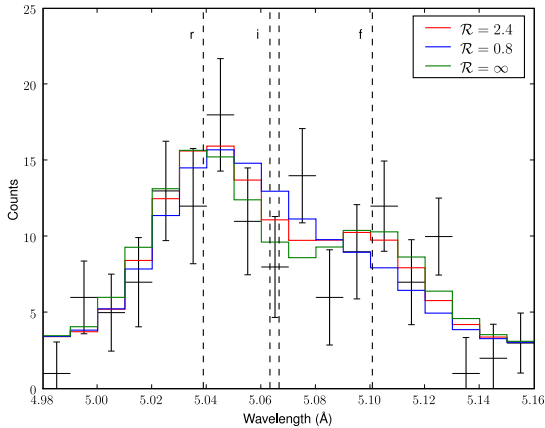


Figure 4. First order MEG spectrum of Cyg OB2 8A (black horizontal lines with error bars) shown near the wavelengths of the S XV triplet together with three models. The positive and negative first orders have been coadded and the spectrum rebinned by a factor of two for presentation purposes. The rest wavelengths of the lines are indicated with dashed vertical lines. The error bars on the individual bins are for presentation purposes and are calculated using the prescription of Churazov et al. (1996). Note that the C statistic (used in this paper) is not computed using a variance function, unlike χ^2 (Cash 1979). The models are from a joint fit with HEG data. The best-fit model is in red, and models with lower and upper limits to the \mathcal{R} parameter at 68% confidence are in blue and green, respectively.

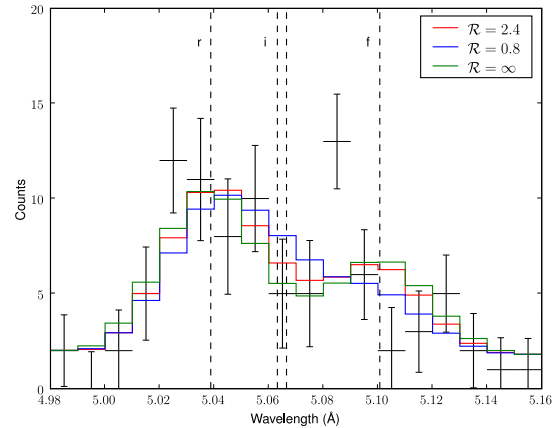


Figure 5. As figure 4, but showing HEG data for S XV in the spectrum of Cyg OB2 8A with models. The positive and negative first orders have been coadded, and the spectrum rebinned by a factor of four for presentation purposes.

symmetric confidence regions reported by WC07. This is true for all the data sets, but it is especially important for the S XV triplet in the spectrum of ζ Pup.

The asymmetry is not surprising, as the dependence of the fit statistic on the line ratio is expected to be nonlinear. As the line ratio becomes very large or very small, the data are no longer very sensitive to changes in the model ratio.

As discussed in § 3.2, it is not clear from the text of the erratum of WC07 how the error bars they reported were derived. However, the symmetry of the error bars reported

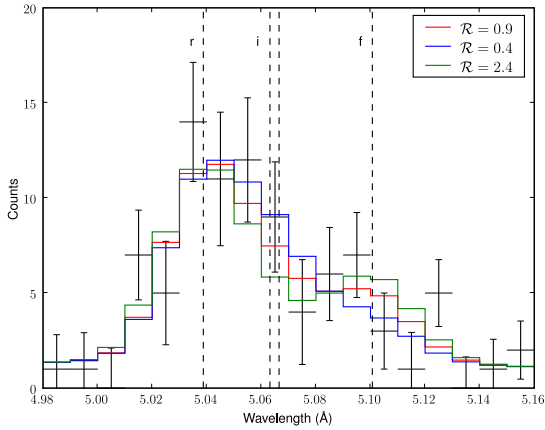


Figure 6. As figure 4, but showing MEG data for S XV in the spectrum of ζ Pup with models. The positive and negative first orders have been coadded, and the spectrum rebinned by a factor of two for presentation purposes.

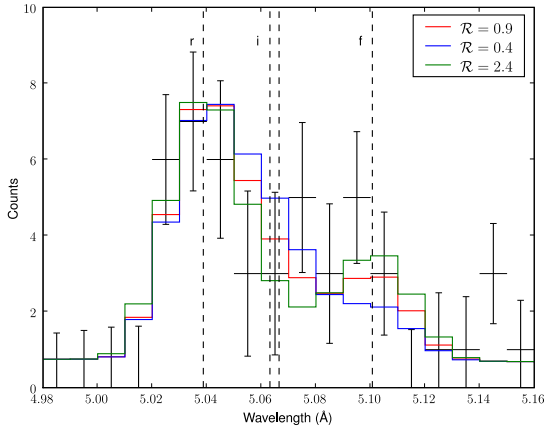


Figure 7. As figure 4, but showing HEG data for S XV in the spectrum of ζ Pup with models. The positive and negative first orders have been coadded, and the spectrum rebinned by a factor of four for presentation purposes.

Table 8. Best-fit Gaussian model for Si XIV in the spectrum of Cyg OB2 8A

σ^a	Δv^b	n^c
850^{+75}_{-100}	-50 ± 100	34 ± 4

^aBest-fit Gaussian velocity width in units of km s^{-1} .

^bBest-fit velocity shift in units of km s^{-1} .

^cBest-fit normalization in units of $10^{-6} \text{ photons cm}^{-2} \text{ s}^{-1}$.

Fit results are for a joint fit to MEG and HEG data. Confidence intervals are reported at 90%.

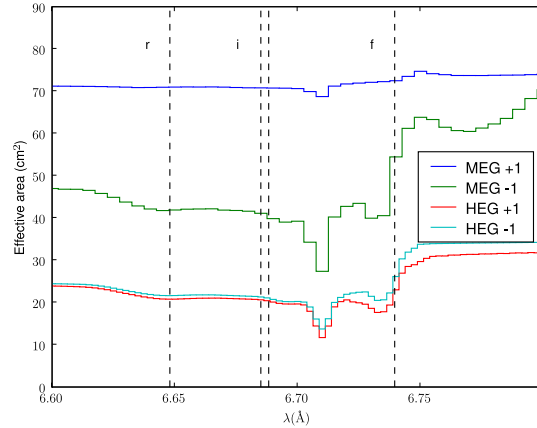


Figure 8. Effective area of individual gratings and orders of HETGS near the wavelengths of the Si XIII triplet for the observation of ζ Per. The rest wavelengths of the triplet are shown with vertical dashed lines. There is a prominent Si K edge near the wavelength of the forbidden line of Si XIII for all the orders which are read out on front-illuminated chips (negative first order MEG, and both first order HEG), but only a small edge for the positive first order MEG, which is read out on a back-illuminated chip.

by WC07 suggests that they may have used a simplified or erroneous procedure for estimation of parameter confidence intervals. It also implies that their procedure did *not* use a delta-fit-statistic criterion to evaluate parameter confidence intervals.

4.6 The Si K edge in the ACIS detector

The effective area of the front-illuminated chips of the ACIS-S detector used in reading out the *Chandra* HETGS shows a strong Si K edge which has significant calibration uncertainties. There is also a Si K edge in the effective area of the back-illuminated chips, but it is much less pronounced.

When using the standard aimpoint for the location of a bright source in the focal plane, the wavelength of the Si K edge falls on a back-illuminated chip for the positive first order MEG data, while it falls on a front-illuminated chip for the negative first order MEG data, as well as both positive and negative first order HEG data. This results in a strong Si K edge in the effective area of all first order HETGS spectra except the MEG positive first order. This is illustrated in Fig 8, where I plot the effective area of all four first order grating arms in the HETGS spectrum of ζ Per in the vicinity of the Si K edge.

The fact that the positive first-order MEG data do not have a strong Si K edge implies that they are the best data for measuring \mathcal{R} for Si XIII, and that if there is any discrepancy between any of the grating orders, the positive first-order MEG data should be considered the most reliable. This is in contradiction to the claim of WC07 that the HEG data have a weaker Si K edge than the MEG data.

4.7 Fits to individual orders: Si XIII in σ Ori and ξ Per

I have measured quite low values for \mathcal{R} in two cases: using only the MEG for Si XIII in the spectrum of σ Ori and using only the HEG for Si XIII in the spectrum of ξ Per. In each of these cases, the joint fit to both the HEG and MEG data gives a much higher value for \mathcal{R} . Both of these measurements to individual gratings agree with the results reported by WC07. Both also disagree at 68% confidence with the results obtained from the same observation, but using the other grating (HEG instead of MEG, or vice versa), although they are formally consistent at 95% confidence. The disagreement between different gratings calls for closer examination.

In order to assess the validity of these measurements I have fit individual grating arms (positive and negative first orders). Although there is in general no reason to expect different results from the individual orders, there are two reasons why this might be useful: first, when looking at positive and negative first order MEG data, uncertainties in the calibration of the strong Si K edge feature in the negative first order MEG data (described in § 4.6) may lead to discrepancies in the two orders; and second, fits to individual orders serve as a consistency check on the results from the joint fit, helping to find artifacts or statistical flukes.

In order to avoid scrutinizing only data for which I have perceived an unexpected outcome, I have performed these fits for *all* data sets considered in this paper. However, I only found significant disagreement between positive and negative first orders for these two cases. I report these fit results in Table 9. The results are also depicted in comparison with those of WC07 in Figure 9.

For the Si XIII data of σ Ori, I find that although the joint fit to the MEG data indicates a quite low value of \mathcal{R} , the two individual grating orders show very different values, although they are formally consistent at the 90% confidence level. The negative first order indicates that \mathcal{R} is relatively small, while the positive first order indicates a much larger value. Since the negative first order may be affected by the strong Si K edge of the front-illuminated CCD chip it falls on, this marginal discrepancy may be resolved by considering the positive first order data as the most reliable, as discussed in § 4.6. Furthermore, the joint fit to the HEG data also indicates a higher value for \mathcal{R} .

For the Si XIII data of ξ Per, I found that the joint best fit to the HEG data required an unrealistically high velocity broadening, such that the lines of the triplet were only marginally resolved from one another. Again, I find that the individual grating orders show very different values of \mathcal{R} , but are formally consistent at the 90% confidence level. However, I also find that the fit to the negative first order HEG data, which prefers a higher value for \mathcal{R} , has a reasonable value for the velocity broadening, which is comparable to the broadening obtained by fitting the MEG data, or to the broadening obtained by fitting lower Z lines (with more counts) in the same spectrum. On the other hand, the fit to the positive first order HEG data, which prefers a low value for \mathcal{R} , requires an unrealistic value for the velocity broadening, as I found for the joint fit. Thus, while there is no reason to prefer one order over the other, it seems reasonable to suppose that the discrepancy between the two orders, combined with the strange velocity distribution of

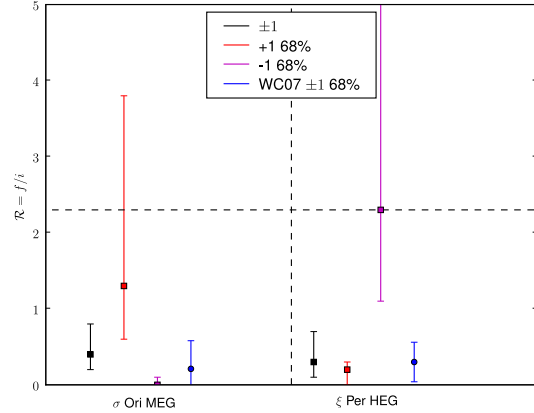


Figure 9. Same as Figure 2, but showing results for individual grating orders for the Si XIII complexes of two specific stars which show discrepancies between orders.

counts in the positive first order HEG data, indicates that these data are either a statistical fluke, or in some other way anomalous. Furthermore, the MEG data are consistent with the hypothesis that $\mathcal{R} = \mathcal{R}_0$. Since the MEG data are unambiguous, and the HEG data show a discrepancy, it is reasonable to conclude that the data are at least as consistent with the hypothesis that $\mathcal{R} = \mathcal{R}_0$ as with any other hypothesis.

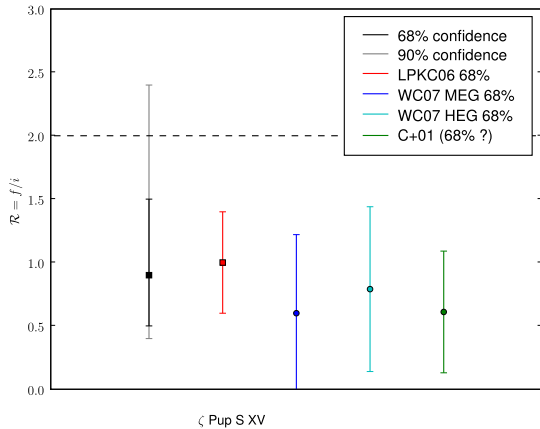
4.8 Constraints on plasma formation radius from the joint fit to Si XIII in the spectrum of ξ Per

Although the constraints on the \mathcal{R} ratio of Si XIII in the spectrum of ξ Per may be skewed by the possibly anomalous positive first order HEG data, as discussed in § 4.7, I will use the formal measurement of \mathcal{R} from the joint fit to MEG and HEG data to derive constraints on the plasma formation radius under the assumption of a single formation radius, in combination with the calculations of Leutenegger et al. (2006). I do this by comparing the measured \mathcal{R} ratios from this work to the plots of $\mathcal{R}(R)$ for ζ Pup and ι Ori in Figures 3 and 5, respectively, of Leutenegger et al. (2006). The photospheric temperature and spectral type of ξ Per is intermediate between those of ζ Pup and ι Ori, so the behavior of \mathcal{R} for ξ Per should be bracketed by that of ζ Pup and ι Ori.

Using the measured 90% confidence limits on the \mathcal{R} ratio of Si XIII in the spectrum of ξ Per ($0.7 < \mathcal{R} < 1.8$), I find an implied plasma location of $2 < R < 6$ using the ζ Pup model UV flux, and $1.4 < R < 4$ using the ι Ori model UV flux. The ranges given here are statistical uncertainties, not plasma distribution ranges. In either case, the data do not require an X-ray emitting plasma located very close to the photosphere. The location inferred is comparable to that inferred for other O stars under the assumption of a single plasma formation radius.

Table 9. Comparison of allowed ranges for \mathcal{R} from fitting individual grating orders in two selected cases

Star	Ion	Grating	best fit	68.3%		90%		95.4%	
				min	max	min	max	min	max
σ Ori	Si XIII	MEG ± 1	0.4	0.2	0.8	0.1	1.3	0.1	1.8
		MEG +1	1.3	0.6	3.8	0.3	12	0.2	∞
		MEG -1	0	0	0.1	0	0.8	0	1.1
ξ Per	Si XIII	HEG ± 1	0.3	0.1	0.7	0.0	1.0	0.0	1.3
		HEG +1	0.2	0.0	0.3	0.0	0.4	0.0	0.6
		HEG -1	2.3	1.1	∞	0.1	∞	0	∞

**Figure 10.** Comparison of results from this work with all previous results on the same data for S XV in the spectrum of ζ Pup. LPKC06 refers to Leutenegger et al. (2006), and C+01 refers to Cassinelli et al. (2001).

4.9 Comparison with previous results for ζ Pup

The S XV triplet of ζ Pup has been studied in several previous works. I compare the previous and current results in Figure 10.

My current results are consistent with the measurements of Leutenegger et al. (2006). It is not possible to comment on the consistency of the results of WC07 and their earlier work, since Cassinelli et al. (2001) did not report which gratings or what confidence intervals were used. Again, while $\mathcal{R} = \mathcal{R}_0$ is ruled out by my measurements at the 68% confidence level, it is allowed at 90%. Thus, these data provide no upper limit on the radial location of the X-ray emitting plasma.

Even using the 68% confidence upper limit of $\mathcal{R} \leq 1.5$, I only infer an upper limit to the radius of S XV of $2.2R_*$ using Figure 3 of Leutenegger et al. (2006) under the assumption of a single plasma formation radius. This limit is completely consistent with the numerical modeling results discussed in the introduction to this paper.

5 DISCUSSION AND CONCLUSIONS

In order to reproduce the measurements of WC07, from which they have inferred the surprising result that hot X-ray emitting plasma is formed very close to photospheres of O

stars, I have measured the $\mathcal{R} = f/i$ ratios of high-Z He-like triplets of several O stars using a simple, robust procedure with an orthodox determination of the 68%, 90%, and 95% confidence intervals. I have used a delta-fit-statistic criterion to compute these confidence intervals, so that model parameter covariance is properly taken into account. In particular, the high-Z He-like triplets are significantly blended, leading to non-negligible covariance in the line normalizations.

I have also shown that, for data of marginal statistical quality, if the centroid shift of the complex is taken as a free parameter, it may be degenerate with the line normalizations. By measuring the centroid shifts of nearby emission lines of good statistical quality, I have shown that it is justified to assume zero centroid shift for the high-Z He-like complexes and remove this degeneracy.

I find that all but one of the complexes considered is consistent with $\mathcal{R} = \mathcal{R}_0$ at 90% confidence, and thus with *no photoexcitation effect*. Since these line complexes are consistent with no photoexcitation, they are thus consistent with plasma located infinitely far away from the star. The one complex that has $\mathcal{R} < \mathcal{R}_0$ is expected based on the strong UV flux of that star, and does not require plasma formation near the photosphere.

Because the data considered in this paper are of poor statistical quality, the location of the X-ray emitting plasma is unconstrained or poorly constrained, and the possibility of X-ray emitting plasma near the photosphere is not excluded in many cases; however, the inference of X-ray emission close to the photosphere would be a surprising result requiring strong positive evidence to establish credibility.

Since there is a large body of evidence indicating that all of the X-ray emitting plasma *other than* the high-Z ions is distributed throughout the winds of O stars, including the velocity broadening of the emission lines and the f/i ratios of low-Z ions (e.g. Waldron & Cassinelli 2001; Kahn et al. 2001; Cassinelli et al. 2001), it would be natural to infer that the high-Z ions are formed in shocks distributed throughout the winds as well, unless there is significant evidence to the contrary. In this work I have shown that the f/i ratios do not constrain these high-Z ions' locations. However, WC07 have shown that in a number of cases high-Z ions inferred by them to be close to the photosphere showed significant velocity broadening, which would not be expected for lines forming very close to the photosphere, where the mean flow velocity is small. I have confirmed their result: many of these lines do indeed show significant velocity broadening, as shown in Table 3. Although WC07 framed the discrepancy between their inferred plasma locations and the large velocity broadenings of the lines as a new, interesting problem, the data

are in fact completely consistent with the hypothesis that the high-Z ions are not forming near the photosphere, but rather in the wind acceleration region, along with the rest of the X-ray emitting plasma.

The fact that the data considered in this paper do not significantly constrain the location of the high-temperature X-ray emitting plasma does not invalidate the conclusion that other He-like triplets *do* provide meaningful constraints (Kahn et al. 2001; Waldron & Cassinelli 2001; Cassinelli et al. 2001; Miller et al. 2002; Waldron et al. 2004; Leutenegger et al. 2006, 2007). However, in all of those cases, lower-Z ions were found to be at locations in the wind that were consistent with a wind-shock origin for the X-ray emitting plasma. Even in the case of θ^1 Ori C, which has a magnetically channeled wind, the X-ray emitting regions may be significantly removed from the photosphere (Gagné et al. 2005).

ACKNOWLEDGMENTS

I would like to acknowledge David Cohen for helpful conversations on statistical techniques and for his careful reading of this manuscript, and David Huenemoerder for help in understanding the calibration of the silicon K edge of the *Chandra* HETGS. I acknowledge support from SAO grant AR7-8002X, NASA grant NNX06AF60G, as well as a fellowship administered by Oak Ridge Associated Universities under the NASA Postdoctoral Program.

REFERENCES

- Blumenthal G. R., Drake G. W. F., Tucker W. H., 1972, *ApJ*, 172, 205
- Canizares C. R., Huenemoerder D. P., Davis D. S., Dewey D., Flanagan K. A., Houck J., Markert T. H., Marshall H. L., Schattenburg M. L., Schulz N. S., Wise M., Drake J. J., Brickhouse N. S., 2000, *ApJ*, 539, L41
- Cash W., 1979, *ApJ*, 228, 939
- Cassinelli J. P., Miller N. A., Waldron W. L., MacFarlane J. J., Cohen D. H., 2001, *ApJ*, 554, L55
- Cassinelli J. P., Olson G. L., 1979, *ApJ*, 229, 304
- Cassinelli J. P., Swank J. H., 1983, *ApJ*, 271, 681
- Churazov E., Gilfanov M., Forman W., Jones C., 1996, *ApJ*, 471, 673
- Cohen D. H., de Messières G. E., MacFarlane J. J., Miller N. A., Cassinelli J. P., Owocki S. P., Liedahl D. A., 2003, *ApJ*, 586, 495
- Cohen D. H., Leutenegger M. A., Grizzard K. T., Reed C. L., Kramer R. H., Owocki S. P., 2006, *MNRAS*, 368, 1905
- Cooper R. G., 1994, Ph.D. Thesis
- Cooper R. G., Owocki S. P., 1994, *Ap&SS*, 221, 427
- Feldmeier A., 1995, *A&A*, 299, 523
- Feldmeier A., Kudritzki R.-P., Palsa R., Pauldrach A. W. A., Puls J., 1997, *A&A*, 320, 899
- Feldmeier A., Puls J., Pauldrach A. W. A., 1997, *A&A*, 322, 878
- Gabriel A. H., Jordan C., 1969, *MNRAS*, 145, 241
- Gagne M., Caillault J.-P., Stauffer J. R., Linsky J. L., 1997, *ApJ*, 478, L87+
- Gagné M., Oksala M. E., Cohen D. H., Tonnesen S. K., ud-Doula A., Owocki S. P., Townsend R. H. D., MacFarlane J. J., 2005, *ApJ*, 628, 986
- Gehrels N., 1986, *ApJ*, 303, 336
- Harnden F. R., Branduardi G., Gorenstein P., Grindlay J., Rosner R., Topka K., Elvis M., Pye J. P., Vaiana G. S., 1979, *ApJ*, 234, L51
- Ignace R., Gayley K. G., 2002, *ApJ*, 568, 954
- Kahn S. M., Leutenegger M. A., Cottam J., Rauw G., Vreux J.-M., den Boggende A. J. F., Mewe R., Güdel M., 2001, *A&A*, 365, L312
- Kramer R. H., Cohen D. H., Owocki S. P., 2003, *ApJ*, 592, 532
- Lampton M., Margon B., Bowyer S., 1976, *ApJ*, 208, 177
- Leutenegger M. A., Owocki S. P., Kahn S. M., Paerels F. B. S., 2007, *ApJ*, 659, 642
- Leutenegger M. A., Paerels F. B. S., Kahn S. M., Cohen D. H., 2006, *ApJ*, 650, 1096
- Lucy L. B., 1982, *ApJ*, 255, 286
- Lucy L. B., White R. L., 1980, *ApJ*, 241, 300
- Macfarlane J. J., Waldron W. L., Corcoran M. F., Wolff M. J., Wang P., Cassinelli J. P., 1993, *ApJ*, 419, 813
- Miller N. A., Cassinelli J. P., Waldron W. L., MacFarlane J. J., Cohen D. H., 2002, *ApJ*, 577, 951
- Mullan D. J., Waldron W. L., 2006, *ApJ*, 637, 506
- Oskinova L. M., Feldmeier A., Hamann W.-R., 2004, *A&A*, 422, 675
- Oskinova L. M., Feldmeier A., Hamann W.-R., 2006, *MNRAS*, 372, 313
- Owocki S. P., Castor J. I., Rybicki G. B., 1988, *ApJ*, 335, 914
- Owocki S. P., Cohen D. H., 1999, *ApJ*, 520, 833
- Owocki S. P., Cohen D. H., 2001, *ApJ*, 559, 1108
- Owocki S. P., Cohen D. H., 2006, *ApJ*, 648, 565
- Porquet D., Mewe R., Dubau J., Raassen A. J. J., Kaastra J. S., 2001, *A&A*, 376, 1113
- Pradhan A. K., 1982, *ApJ*, 263, 477
- Press W. H., Teukolsky S. A., Vetterling W. T., Flannery B. P., 2007, *Numerical recipes. The art of scientific computing*. Cambridge: University Press, —c2007, 3rd ed.
- Runacres M. C., Owocki S. P., 2002, *A&A*, 381, 1015
- Seward F. D., Forman W. R., Giacconi R., Griffiths R. E., Harnden F. R., Jones C., Pye J. P., 1979, *ApJ*, 234, L55
- Waldron W. L., Cassinelli J. P., 2001, *ApJ*, 548, L45
- Waldron W. L., Cassinelli J. P., 2007, *ApJ*, 668, 456
- Waldron W. L., Cassinelli J. P., Miller N. A., MacFarlane J. J., Reiter J. C., 2004, *ApJ*, 616, 542